Probing Wrapping Dynamics of Spherical Nanoparticles by 3D Vesicles Using Force-based Simulations

Didarul Ahasan Redwan[1], Ke Du[2], Xin Yong[1*]
[1] Department of Mechanical Engineering, Binghamton University, Binghamton, NY 13902, USA.
[2] Department of Chemical and Environmental Engineering, University of California Riverside, Riverside, California 92521, United States
*Email: xyong@binghamton.edu

Supplementary Information

1. Benchmark geometric properties calculation for discretized surfaces

Calculation of local mean curvature $H(\mathbf{x})$ and Laplacian of the mean curvature $\Delta_s H(\mathbf{x})$ (which is a fourth-order derivative) is central to the evaluation of bending energy and force. We assess the accuracy of our method for computing these geometric quantities on triangulated surfaces using the representative shape of red blood cells (RBCs), depicted in Figure S1. The analytical expression of this biconcave shape is given by

$$z = \pm\frac{R}{2}\sqrt{1-r^2}(C_0 + C_1 r^2 + C_2 r^4)$$

Here, $r = \sqrt{x^2+y^2}/R$ is the normalized projected radial distance, with R being the length of the large half-axis of the RBC. The values for the constants C_0, C_1 and C_2 are 0.2072,2.0026, and -1.1228, respectively.[1] To make the curvature dimensionless, we set $R = 1$ in the test. With this analytical expression, the geometric properties of this surface can be theoretically calculated by differential geometry, enabling the comparison with those calculated on the triangulated surface. The numerical and analytical results have been plotted as functions of the polar angle θ_i, which is defined as follows:

$$\theta_i = \arccos\frac{z_i}{\sqrt{x_i^2 + y_i^2 + z_i^2}}$$

Here, x_i, y_i, and z_i are the Cartesian coordinates of the vertex i of the discretized surface. The relative errors for each vertex $\mathbf{x}_i$ are given by the normalized Euclidean norms:[2]

$$\varepsilon_H(\theta_i) = \frac{\left|H^{\text{analytical}}(\mathbf{x}_i) - H^{\text{numerical}}(\mathbf{x}_i)\right|}{\max\left|H^{\text{analytical}}\right|}$$

$$\varepsilon_{\Delta H}(\theta_i) = \frac{\left|\Delta_s H^{\text{analytical}}(\mathbf{x}_i) - \Delta_s H^{\text{numerical}}(\mathbf{x}_i)\right|}{\max\left|\Delta_s H^{\text{analytical}}\right|}$$

where H and $\Delta_s H$ are normalized by the maximum absolute values of the mean curvature and the Laplacian of the mean curvature on the entire surface. Figure S2 shows that the maximal error of the mean curvature does not converge as mesh density increases, while the average relative error follows a second-order convergence. The fourth-order quantity, the Laplacian of the mean curvature, fails to converge even for the average relative error, retaining a systematic deviation. Our results are consistent with previous reports.[2]

2. Validation of vesicle shape transformation

We performed a comprehensive validation of our model by reproducing previously observed phase diagrams of vesicle shapes. The bending modulus κ_b, volume modulus κ_v, and area modulus κ_a were set to 0.01, 2.0, and 1.0, respectively. The preferred surface area A_0 was set to the surface area of a unit sphere 4π. The preferred vesicle volume is calculated according to the reduced volume, which is the ratio of the vesicle volume V to the volume of a sphere with the same surface area A, $v = 6\sqrt{\pi}V/A^{3/2}$. The total volume of a vesicle can be defined as $V = \sum_t^{N_T} V^t$, where V^t is the volume of the tetrahedron formed by triangle t and an arbitrary point (selected as the origin here) and N_T is the total number of triangles of the mesh. This volume is calculated by the following formula:[3]

$$V^t = \frac{1}{3}A^t h$$

Here, A^t is the area of triangle t and h is the corresponding height of the tetrahedron. The total area of the membrane surface is computed by summing up areas of all triangles:

$$A = \sum_t^{N_T} A^t$$

The initial vesicle shapes were selected as oblate and prolate spheroids.

Figure S3 presents the energy curves following different reduced volumes for initial oblate and prolate vesicle configurations. This diagram delineates the normalized bending energy of the vesicles in relation to the reduced volume. Notably, the phase diagram we derived from vesicle shape optimization aligns closely with theoretical predictions in both energy and shapes. Figure S4 showcases the final equilibrium shapes of both prolate and oblate branches for v ranging from 0.6 to 1.0. For the prolate branch, the vesicle elongates as the reduced volume decreases. When v reaches 0.67, the vesicle adopts a dumbbell shape. Further reductions in volume lead to the emergence of metastable states.[4] In contrast, vesicles initially shaped as oblates flatten as v decreases and transition to a biconcave form when the reduced volumes lie between 0.59 and 0.65. Crucially, it is observed that a single target reduced volume can yield two distinct, locally minimized energy states, contingent on the initial shape of the vesicle.

References

1. Evan Evans and Yuan-Cheng Fung. Improved measure of the erythrocytegeometry. Microvascular research, 4(4):335–347, 1972
2. Achim Guckenberger and Stephan Gekle. Theory and algorithms to compute helfrich bending forces: A review. Journal of Physics: Condensed Matter, 29(20):203001, 2017.
3. Keenan Crane and Max Wardetzky. A glimpse into discrete differential geometry. Notices of the American Mathematical Society, 64(10), 2017.
4. Xin Bian, Sergey Litvinov, and Petros Koumoutsakos. Bending models of lipid bilayer membranes: Spontaneous curvature and area-difference elasticity. Computer Methods in Applied Mechanics and Engineering, 359:112758, 2020.

5. Udo Seifert, Karin Berndl, and Reinhard Lipowsky. Shape transformations of vesicles: Phase diagram for spontaneous curvature and bilayer-coupling models. Physical review A, 44(2):1182, 1991.

Supplementary Figures

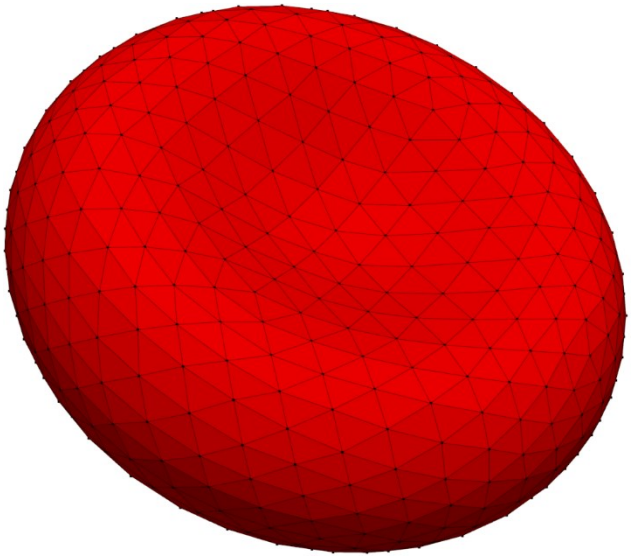

Figure S1. A discretized biconcave shape with 1280 triangles.

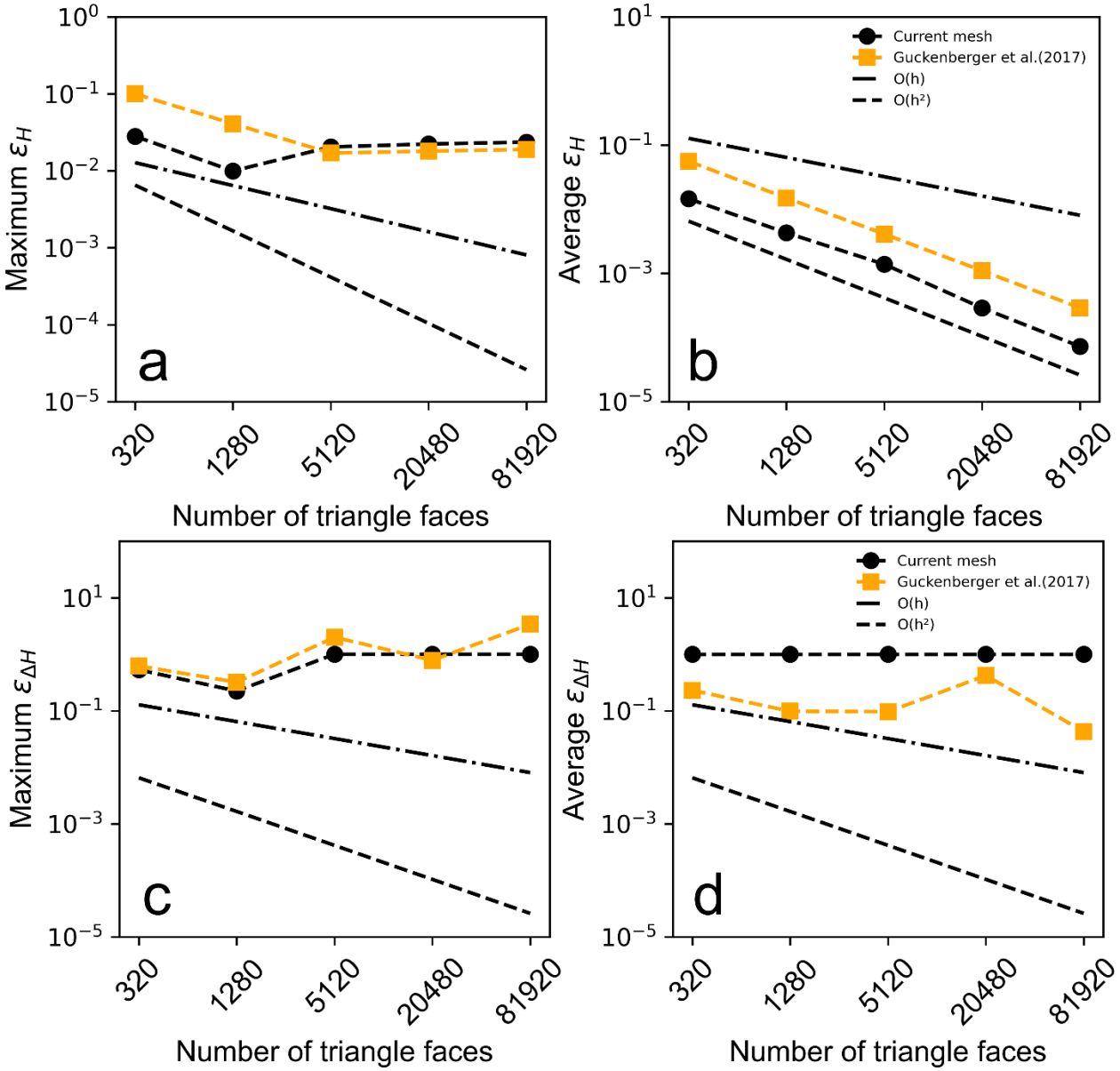

Figure S2. (a) Maximum and (b) average relative errors for the mean curvature. (c) Maximum and (d) average relative errors for the Laplacian of the mean curvature.

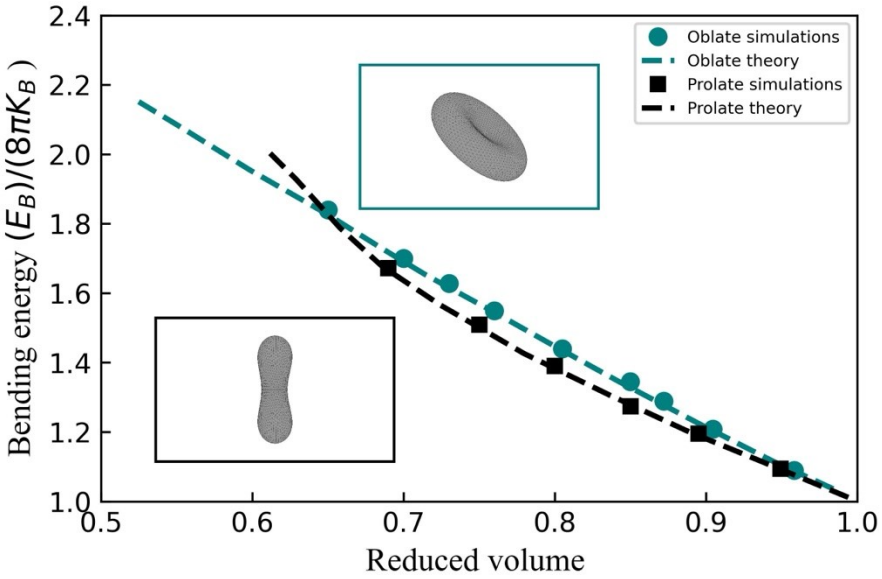

Figure S3. Minimized energy states at different reduced volumes for vesicles with the oblate and prolate spheroids as the initial shapes. The number of triangles of the mesh is 5120. The dashed lines represent the theoretical results adapted from Ref. 5. The insets show representative dumbbell and biconcave shapes of vesicles at low reduced volume.

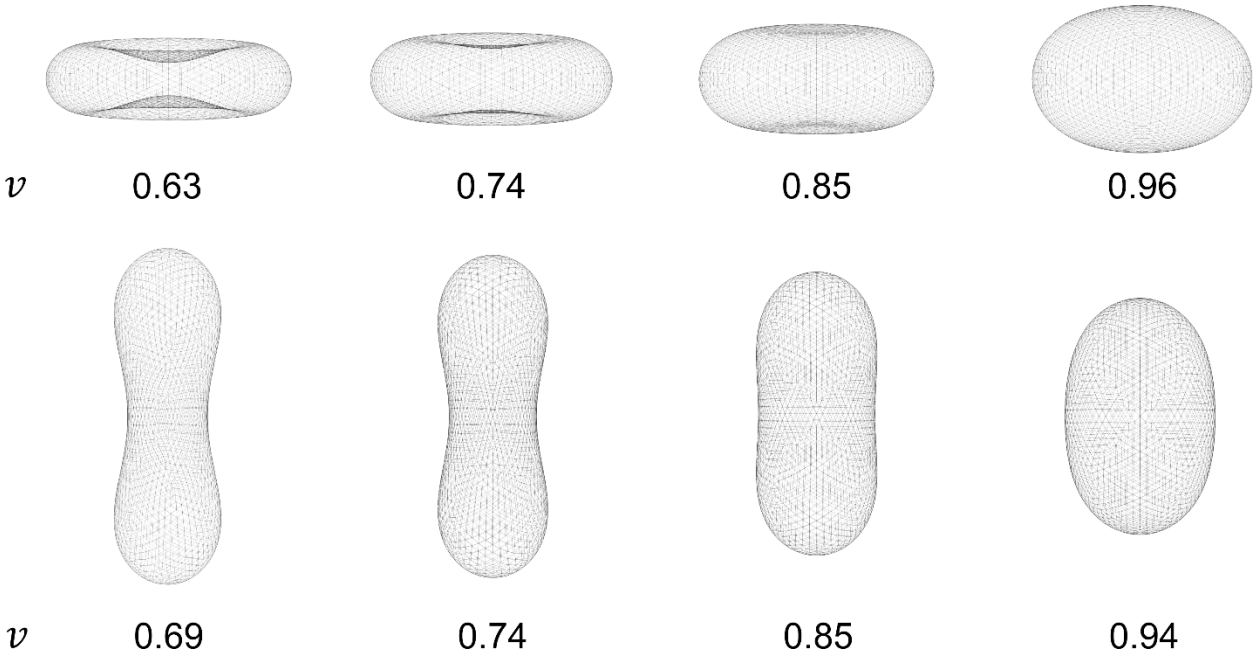

Figure S4. Equilibrium shapes of vesicles at different reduced volumes with the oblate (top) and prolate (bottom) spheroids as the initial shapes.

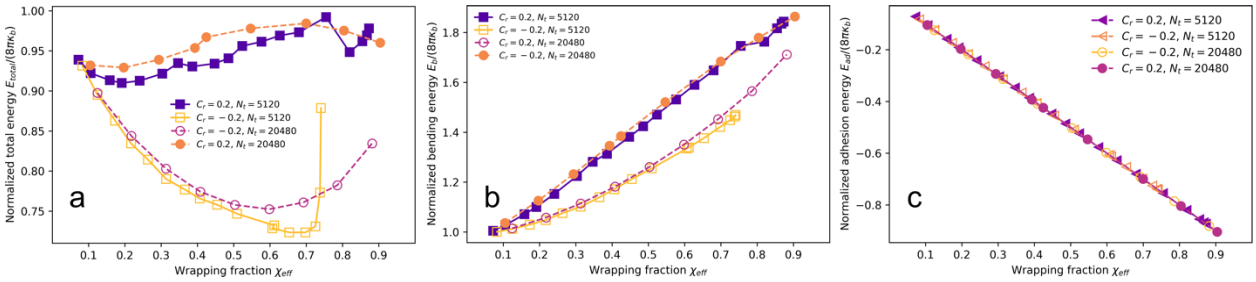

Figure S5. Normalized (a) total, (b) bending and (c) adhesion energies of spherical vesicles having two different mesh densities (5120 and 20480 triangles) interacting with a single nanoparticle of relative curvature $C_r = \pm 0.2$ at different effective wrapping fractions. The solid and open symbols represent the states with particles located outside and inside the vesicle, respectively.

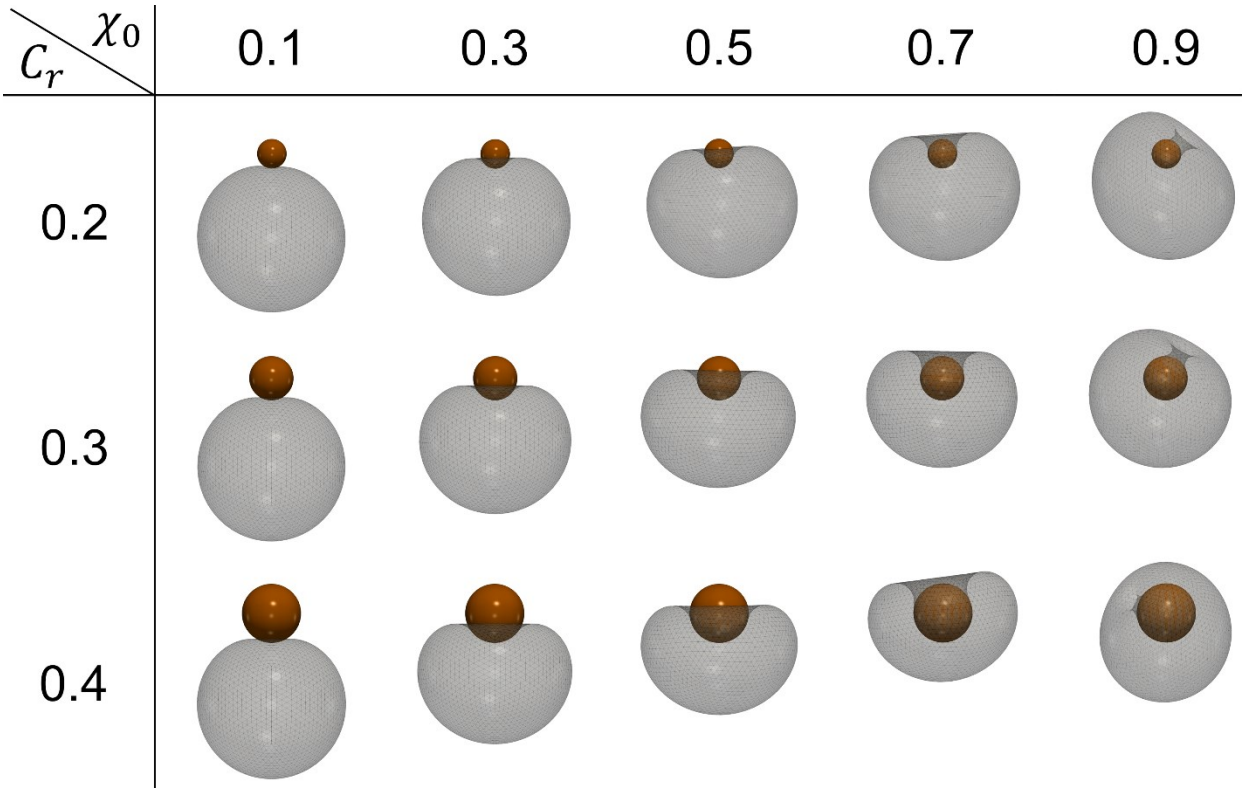

Figure S6. An array of equilibrium snapshots of single particle interaction with spherical fluid vesicle for different positive relative curvatures (outside particle) and target wrapping fractions. The vesicle mesh is composed of 5120 triangles.

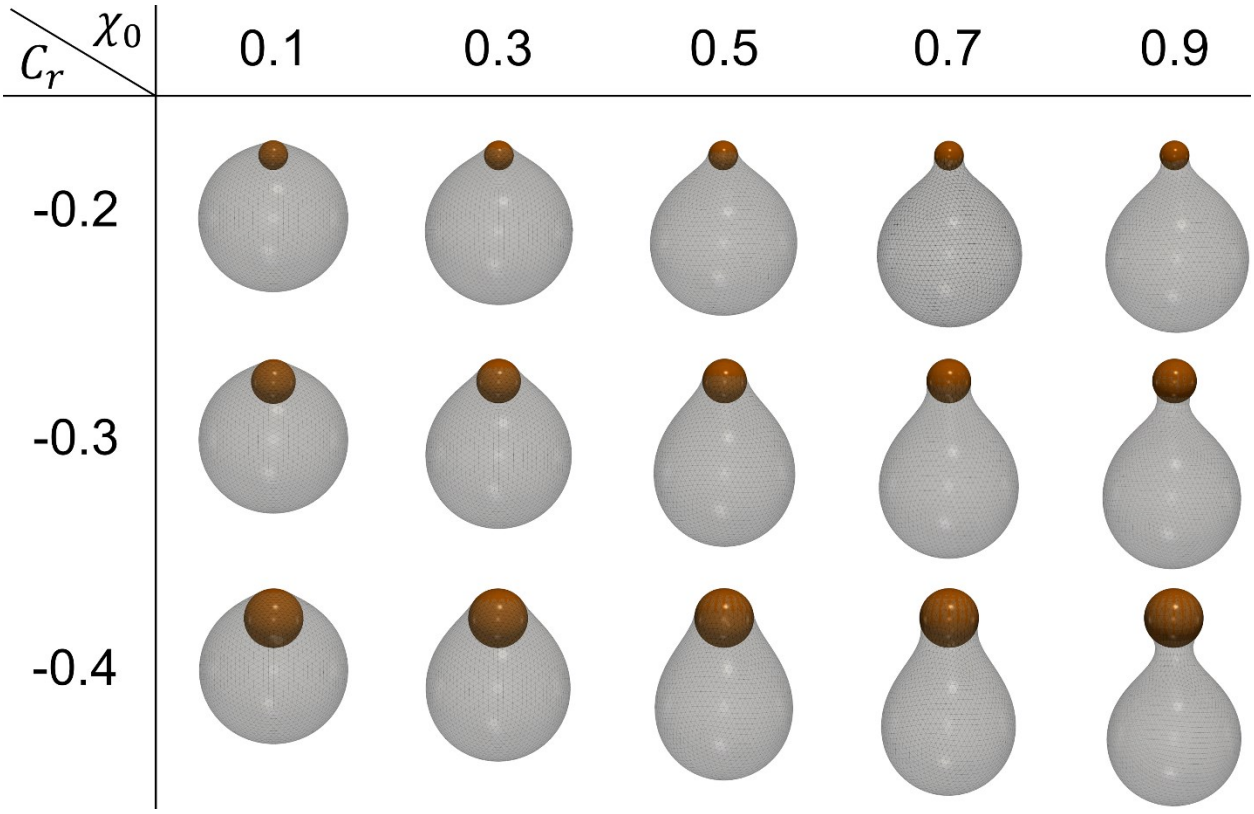

Figure S7. An array of equilibrium snapshots of single particle interaction with spherical fluid vesicle for different negative curvatures (inside particle) and target wrapping fractions. The vesicle mesh is composed of 5120 triangles.

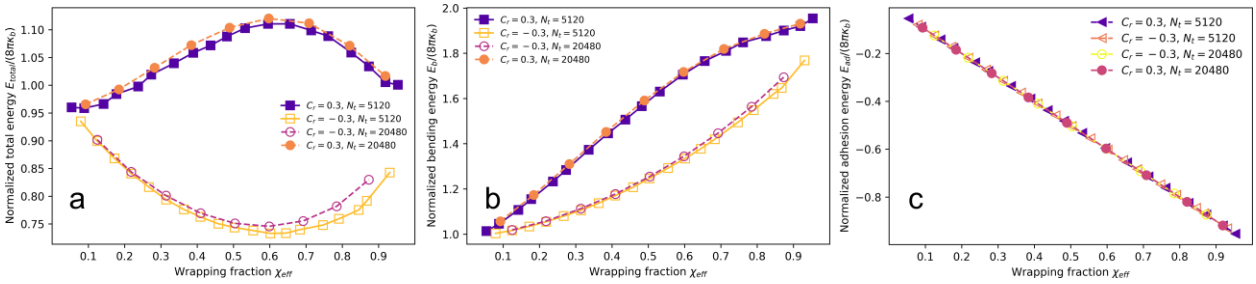

Figure S8. Normalized (a) total, (b) bending and (c) adhesion energies of spherical vesicles having two different mesh densities interacting with a single nanoparticle of relative curvature $C_r = \pm 0.3$ at different effective wrapping fractions. The solid and open symbols represent the states with particles located outside and inside the vesicle, respectively.

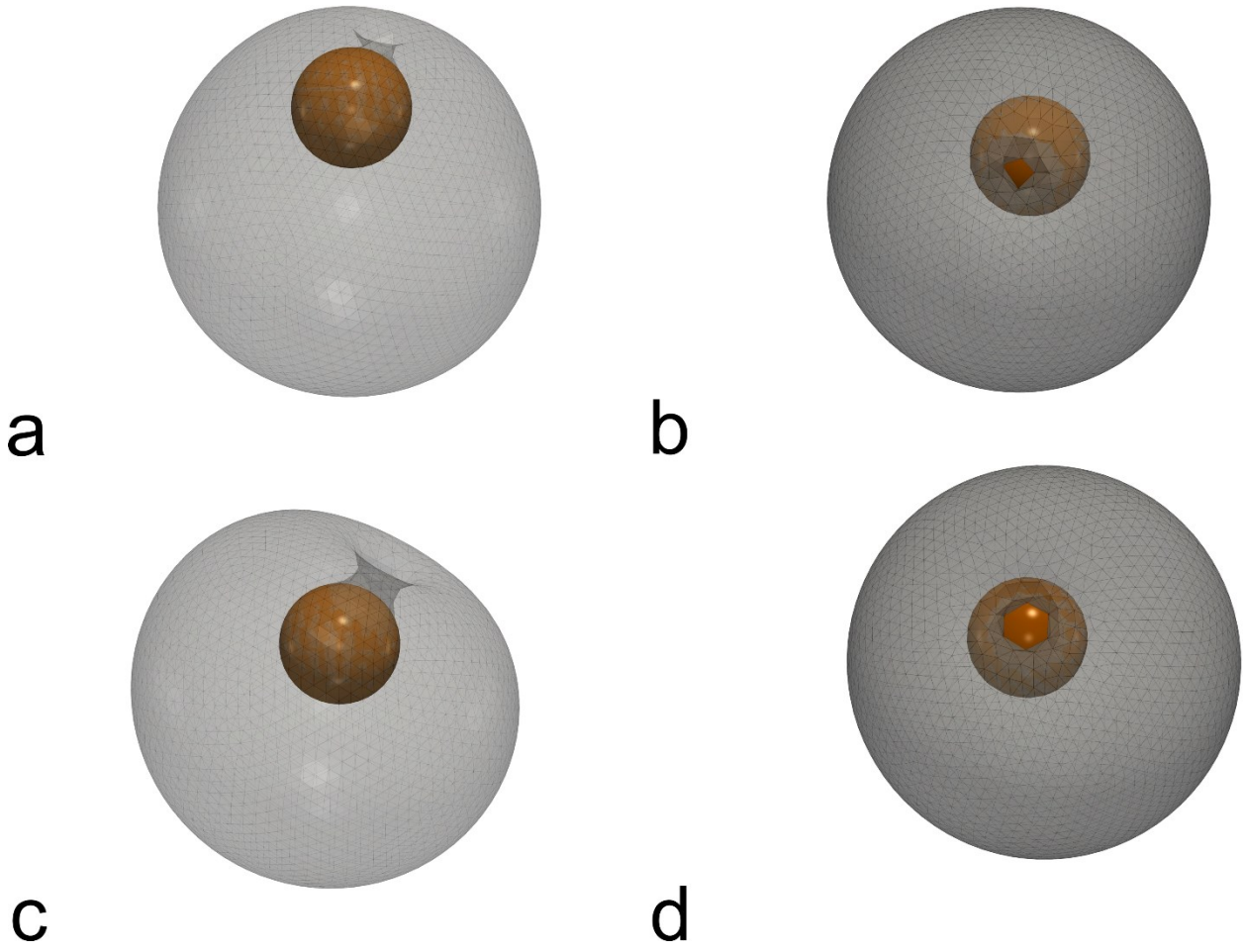

Figure S9. Detailed views of (a) representative intermediate wrapping state and (b) unstable neck morphology for external particle wrapping at target wrapping fraction χ_0 of 0.9 and relative curvature C_r of 0.3. The final equilibrium (c) wrapping state and (d) neck morphology are also depicted for comparison. The number of triangles of the vesicle is 5120. The brown color indicates the particles with the bias potential.

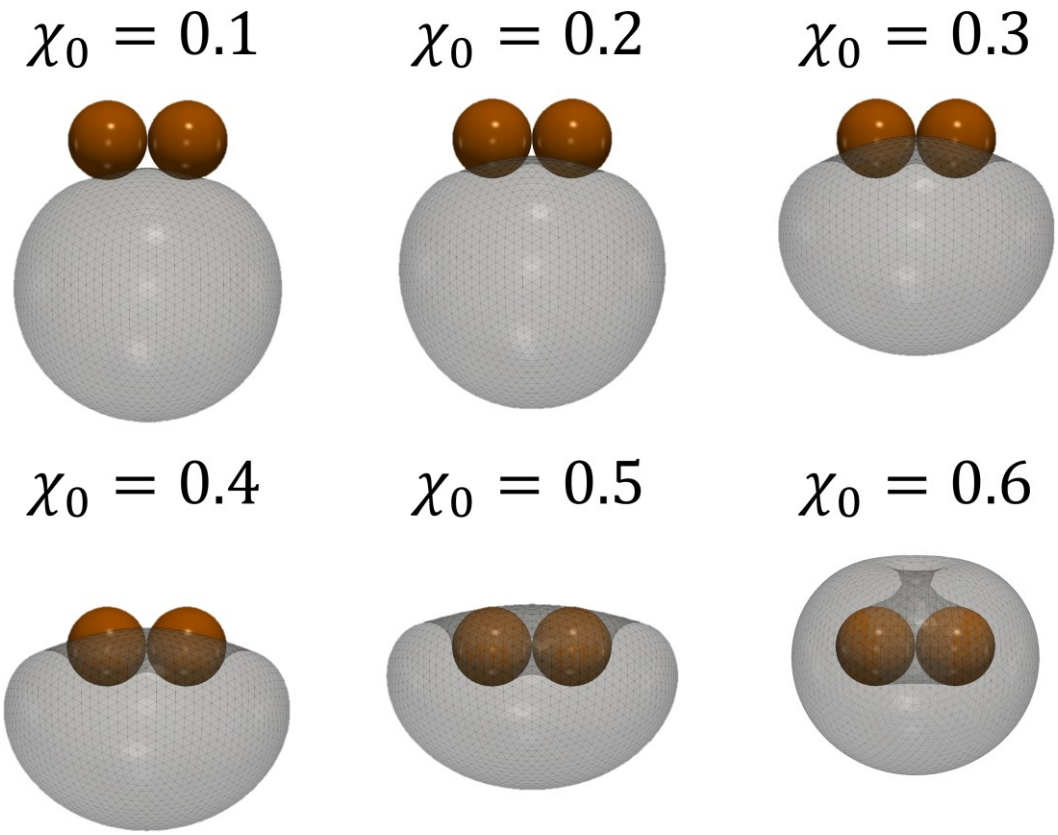

Figure S10. Final equilibrium snapshots of two adjacent particles having a relative curvature C_r of 0.3 interacting with a spherical vesicle from outside at different target wrapping fractions.

Supplementary Videos

Movie S1. Single nanoparticle interaction with a biconcave-shaped vesicle from the top concave region with no biasing potential (red particle).

Movie S2. Simultaneous interaction of two nanoparticles with a biconcave-shaped vesicle from the top and bottom of the biconcave region with no biasing potential (red particles).

Movie S3. Simultaneous interaction of two nanoparticles with a biconcave-shaped vesicle from the convex “waist” region with a biasing potential with a target wrapping fraction of 0.5 (brown particles).